INVITED PAPER *Special Section on 2007 International Symposium on Antennas and Propagation*

Antenna Design for Mobile MIMO Systems

Michael JENSEN[†a)], **Britton QUIST**[†], *and* **Nicolas BIKHAZI**[†], *Nonmembers*

SUMMARY While significant work has been dedicated to analyzing the performance of antennas for multiple-input multiple-output (MIMO) and diversity systems, little has appeared on synthesizing optimal antennas for these systems. This paper explores optimal antenna characteristics given understanding about the average structure of the propagation environment, making the results applicable for time-varying channels created by mobile nodes or scatterer motion. Specifically, it examines optimal antenna designs for the cases where 1) the antennas reside in a fixed aperture or 2) the number of antenna elements is fixed (under fast-fading conditions with spatially correlated signals).

key words: *MIMO systems, antennas*

1. Introduction

Numerous analytical and experimental studies have revealed the dramatic capacity increase enabled by exploiting the multipath spatial structure with multiple-input multiple-output (MIMO) wireless communications and have demonstrated the impact of the antenna radiation characteristics on the resulting performance [1]. However, specific work on the *synthesis* of antennas for MIMO systems has been largely limited to the common rule-of-thumb that radiation pattern orthogonality generally leads to good performance [2], [3]. While this is a useful notion, what is lacking is a generalization of this concept which can specify optimal antenna radiation characteristics given basic information about the propagation environment.

While some work on this topic has generated optimal MIMO antenna properties for specific channels [4], [5], the resulting characteristics are not guaranteed to be optimal in an average sense as the channel changes, such as might occur for mobile nodes or time-varying scatterers. Furthermore, these approaches necessarily consider the transmit and receive antenna characteristics together (i.e. the designs are interdependent), whereas an effective and practical approach for antenna synthesis should rely only on *average* propagation behavior at one end of the link.

This paper proposes a method for determining the optimal antenna array radiation characteristics based on stochastic characteristics of the propagation environment at either the transmit or receive end of the link under two different scenarios. In the first scenario, the optimal antenna currents and radiation patterns are derived based on knowledge of the power angular spectrum (PAS) for the environment assuming the antennas are constrained to lie within a *fixed aperture*. The performance of the optimal antennas is also compared to that obtained with practical designs synthesized using genetic algorithm optimization [6]. The second scenario examines the problem of antenna synthesis for a *fixed number of antennas* under the assumptions of highly mobile nodes, with specific focus on recent findings that under these circumstances decreased antenna array spacing monotonically increases the resulting system performance [7]. This paper shows that this behavior is associated with increased power radiated by the transmit array and demonstrates that when the radiated power is explicitly limited, the capacity is maximized at a non-zero antenna spacing as expected.

Manuscript received November 25, 2007.
Manuscript revised February 5, 2008.

[†]The authors are with the Department of Electrical and Computer Engineering, Brigham Young University, Provo, UT, USA.
a) E-mail: jensen@ee.byu.edu

DOI: 10.1093/ietcom/e91–b.6.1705

2. Optimal Antennas for a Fixed Aperture

The goal of this section is to identify the antenna characteristics that optimize the *average* performance of MIMO and diversity systems in time-varying propagation channels. Because such a notion fits well within the framework of analysis of antenna diversity performance, we will use diversity gain as a performance measure. Since antennas that enable good diversity performance generally also enable good MIMO performance [1], such an approach appears reasonable.

The analysis uses boldface lowercase and uppercase symbols to denote column vectors (vector $\mathbf{x}$ with nth element x_n) and matrices (matrix $\mathbf{A}$ whose element in the mth row and nth column is A_{mn}) respectively. Vectors which represent an electromagnetic field or radiation pattern or coordinates in space have an overbar ($\overline{\mathbf{e}}$), and dyads have two overbars ($\overline{\overline{\mathbf{P}}}$).

2.1 Signal Covariance

Consider a scenario where a vector field $\overline{\mathbf{p}}_{\text{inc}}(\Omega)$ impinges on an antenna confined to the volume V, where Ω is used here to represent an angular position in spherical coordinates or $\Omega = (\theta, \phi)$, with θ and ϕ representing respectively elevation and azimuthal angles. We assume that the field is a zero-mean complex Gaussian stochastic process with the field arriving at one angle uncorrelated with that arriving at another angle, or

$$\mathrm{E}\left\{\overline{\mathbf{p}}_{\text{inc}}(\Omega)\overline{\mathbf{p}}^{\dagger}_{\text{inc}}(\Omega')\right\} = \overline{\overline{\mathbf{P}}}(\Omega)\delta(\Omega - \Omega'), \tag{1}$$

where $\mathrm{E}\{\cdot\}$ represents an expectation, $\{\cdot\}^\dagger$ is the conjugate transpose, $\delta(\cdot)$ is the Dirac delta function, and $\overline{\overline{\mathbf{P}}}(\Omega) = \mathrm{E}\left\{\overline{\mathbf{p}}_{\mathrm{inc}}(\Omega)\overline{\mathbf{p}}^{\dagger}_{\mathrm{inc}}(\Omega)\right\}$ is the dyadic PAS of the incident field. This dyadic form contains the average power in each polarization (diagonal elements) and the cross-correlation of the different polarizations (off-diagonal elements).

Using this representation, if $\overline{\mathbf{e}}_m(\Omega)$ represents the open-circuit electric field radiation pattern of the mth receive antenna, then the open-circuit voltage on this antenna can be written as [3]

$$v_m = \varphi \int_\Omega \overline{\mathbf{e}}_m(\Omega) \cdot \overline{\mathbf{p}}_{\mathrm{inc}}(\Omega)\, d\Omega, \tag{2}$$

where φ is a constant. Since this is simply a linear operation on a zero-mean complex Gaussian random vector, the resulting voltage will also be a zero-mean complex Gaussian random variable [8]. The covariance matrix $\mathbf{R}$ for the antenna terminal voltage signals has elements

$$\begin{aligned} R_{mp} &= \mathrm{E}\left\{v_m v_p^*\right\} \\ &= |\varphi|^2 \int_\Omega \overline{\mathbf{e}}_m(\Omega) \cdot \overline{\overline{\mathbf{P}}}(\Omega) \cdot \overline{\mathbf{e}}_p^*(\Omega)\, d\Omega, \end{aligned} \tag{3}$$

where $\{\cdot\}^*$ is a conjugate and we have used (1) along with the fact that $\overline{\mathbf{e}}_m(\Omega)$ is deterministic.

This covariance matrix is a key quantity which contains the information necessary to determine the diversity performance of the antenna array in the environment. In fact, a key contribution of the work reported in [2] is that the diversity gain of a system with correlated antennas may be computed by creating an equivalent system of uncorrelated antennas with the branch gains given by the eigenvalues of the covariance matrix. Optimal antennas, therefore, will physically create the scenario where the diagonal elements of $\mathbf{R}$ are large (indicating large received power) and the off-diagonal elements are small (indicating low correlation). Note that under the condition $\overline{\overline{\mathbf{P}}}(\Omega) = \overline{\overline{\mathbf{I}}}$ (incident power uniformly distributed in angle), this means that the radiation patterns are orthogonal, consistent with traditional design goals.

2.2 Basis Expansion

The first step in this formulation is to relate the radiation patterns used in (3) to the physical aperture to which the antennas are restricted. Patterns can be defined either by considering radiating currents (transmit perspective) or the weighting of the fields incident on the aperture (receive perspective), with reciprocity relating the two perspectives. While our development of the covariance has used received incident fields, it is arguably more intuitive to define the radiation patterns in terms of radiating currents.

Therefore, consider an electric current distribution residing in our volume V consisting of a weighted sum of vector functions $\overline{\mathbf{j}}_m(\overline{\mathbf{r}})$, with the radiation pattern for the mth current function being given by [9]

$$\overline{\mathbf{e}}_m(\Omega) = \int_V \overline{\overline{\mathbf{G}}}(\Omega, \overline{\mathbf{r}}) \cdot \overline{\mathbf{j}}_m(\overline{\mathbf{r}})\, d\overline{\mathbf{r}}, \tag{4}$$

where $\overline{\overline{\mathbf{G}}}(\Omega, \overline{\mathbf{r}})$ is the dyadic Green's function relating the currents to the far-field radiation. To facilitate determination of the current functions which create the optimal radiation patterns, we represent the mth current function as a weighted sum of orthonormal vector basis functions $\overline{\mathbf{f}}_n(\overline{\mathbf{r}})$, or

$$\overline{\mathbf{j}}_m(\overline{\mathbf{r}}) = \sum_n B_{nm} \overline{\mathbf{f}}_n(\overline{\mathbf{r}}), \tag{5}$$

where B_{nm} represents an unknown weighting coefficient. Substitution of this expansion into (4) yields

$$\overline{\mathbf{e}}_m(\Omega) = \sum_n B_{nm} \underbrace{\int_V \overline{\overline{\mathbf{G}}}(\Omega, \overline{\mathbf{r}}) \overline{\mathbf{f}}_n(\overline{\mathbf{r}})\, d\overline{\mathbf{r}}}_{\overline{\mathbf{z}}_n(\Omega)}, \tag{6}$$

where the function $\overline{\mathbf{z}}_n(\Omega)$ represents the radiation pattern of the nth basis function. Use of this result in (3) gives

$$\mathbf{R} = \mathbf{B}^T \mathbf{C} \mathbf{B}^*, \tag{7}$$

where $\{\cdot\}^T$ represents a transpose and

$$C_{nq} = \int_\Omega \overline{\mathbf{z}}_n(\Omega) \cdot \overline{\overline{\mathbf{P}}}(\Omega) \cdot \overline{\mathbf{z}}_q^*(\Omega)\, d\Omega. \tag{8}$$

2.3 Constraints

Before determining the unknown coefficients contained in $\mathbf{B}$, we must first impose constraints on the solution. The first is that all radiation patterns should be normalized so that they have the same radiated power, or

$$\frac{1}{2\eta_0} \int \overline{\mathbf{e}}_m^*(\Omega) \cdot \overline{\mathbf{e}}_m(\Omega)\, d\Omega = P_{\mathrm{rad}}, \tag{9}$$

where P_{rad} is the desired total radiated power for each pattern and η_0 is the free-space intrinsic impedance. If the vector $\mathbf{b}_m$ represents the mth column of the matrix $\mathbf{B}$, then using (6) in (9) leads to

$$\mathbf{b}_m^\dagger \mathbf{A} \mathbf{b}_m = P_{\mathrm{rad}}, \tag{10}$$

where

$$A_{nq} = \frac{1}{2\eta_0} \int \overline{\mathbf{z}}_n^*(\Omega) \cdot \overline{\mathbf{z}}_q(\Omega)\, d\Omega. \tag{11}$$

We recognize that since the coefficients in $\mathbf{b}_m$ represent currents, $\mathbf{A}$ represents the real part of the full impedance matrix for the array [10].

Next, we recognize that general current distributions can lead to supergain which is impractical [10], [11], motivating development of a constraint that limits the level of supergain allowable in the solution. We will use the approach developed in [10] where a small loss resistance $R_{L,n}$ is associated with the nth basis function and used as the nth diagonal element of a diagonal matrix $\mathbf{R}_L$. This leads to a

redefinition of the resistance matrix as $\widehat{\mathbf{A}} = \mathbf{A} + \mathbf{R}_L$ and the modification of (10) to constrain the power *delivered* to the array, or $\mathbf{b}_m^\dagger \widehat{\mathbf{A}} \mathbf{b}_m = P_\mathrm{d}$.

The loss in the formulation must be specified in a physically meaningful way. If the basis functions used are square-integrable, then one method for specifying the loss is assuming that the currents flow in a material with a conductivity of σ_L. The loss resistance associated with the nth basis is then given by

$$R_{L,n} = \frac{1}{\sigma_L} \int_V |\overline{\mathbf{f}}_n(\overline{\mathbf{r}})|^2 \, d\overline{\mathbf{r}}, \tag{12}$$

where $|\cdot|$ represents the vector magnitude. Generally, we will use basis functions which all have the same value of loss resistance when computed using (12).

When the formulation uses dipoles (approximated by delta functions such that (12) cannot be used), it is convenient to specify the radiation efficiency of the nth dipole defined as $\mu_n = A_{nn}/(A_{nn} + R_{L,n})$ so that $R_{L,n} = A_{nn}(1/\mu_n - 1)$. For identical dipoles, $A_{nn} = A_{11}$ and therefore we typically choose $R_{L,n}$ to be the same for all n.

2.4 Solution

We seek the vector $\mathbf{b}_m$ which maximizes the quadratic $\mathbf{b}_m^T \mathbf{C} \mathbf{b}_m^*$ subject to the delivered power constraint. Using the transformation $\mathbf{b}_m = P_\mathrm{d}^{1/2} \widehat{\mathbf{A}}^{-1/2} \mathbf{d}_m$, we can formulate this as a Lagrange multiplier problem [12] of the form

$$\mathbf{d}_m = \max_{\mathbf{d}_m} \left\{ P_\mathrm{d} \mathbf{d}_m^\dagger \widehat{\mathbf{C}} \mathbf{d}_m + \gamma_m P_\mathrm{d} (1 - \mathbf{d}_m^\dagger \mathbf{d}_m) \right\}, \tag{13}$$

where γ_m represents the Lagrange multiplier, $\widehat{\mathbf{C}} = \widehat{\mathbf{A}}^{-1/2} \mathbf{C}^T \widehat{\mathbf{A}}^{-1/2}$, and we have used the fact that the first term is a scalar so that we can take its transpose.

To find the maximizing solution, we take the variation of the argument in (13) with respect to $\mathbf{d}_m$ and set it equal to zero [12], which after simplification leads to $\mathbf{d}_m^\dagger (\widehat{\mathbf{C}} - \gamma_m \mathbf{I}) = 0$. Since $\widehat{\mathbf{C}}$ is Hermitian, this implies that $(\widehat{\mathbf{C}} - \gamma_m^* \mathbf{I}) \mathbf{d}_m = 0$, indicating that γ_m^* is a (real) eigenvalue of $\widehat{\mathbf{C}}$ with $\mathbf{d}_m$ the corresponding eigenvector. Writing $\widehat{\mathbf{C}} = \boldsymbol{\xi} \boldsymbol{\Lambda} \boldsymbol{\xi}^\dagger$ and $\mathbf{B} = P_\mathrm{d}^{1/2} \widehat{\mathbf{A}}^{-1/2} \boldsymbol{\xi}$, where $\boldsymbol{\xi}$ and $\boldsymbol{\Lambda}$ represent respectively the unitary matrix of eigenvectors and diagonal matrix of eigenvalues of $\widehat{\mathbf{C}}$, leads to $\mathbf{R} = P_\mathrm{d} \boldsymbol{\Lambda}$ which is diagonal as desired. This is an intriguing result, since the actual Lagrange multiplier problem was not formulated to ensure diagonalization of this matrix. Furthermore, since the covariance represents the M eigenvalues of a matrix, then if we desire to limit ourselves to $\widehat{M} \le M$ actual antennas, choosing the eigenvectors corresponding to the $\widehat{M}$ largest eigenvalues will lead to the largest possible values of the diagonal covariance matrix elements.

2.5 Example Computations

We consider a set of vertically-oriented (z-oriented) dipoles arranged in a regular grid in the x-y plane bounded by a square of side length 1λ, where λ represents the free-space wavelength. To create the array, we subdivide the square aperture into a regular grid of square cells, with 11 cells in each dimension, and place the vertically-oriented dipoles at the center of each cell. We compute the value of A_{nn} for the nth dipole, and then choose the loss resistance such that the radiation efficiency μ_n achieves the specified value. We further assume that the incident field is vertically polarized with propagation confined to the horizontal plane, or

$$\overline{\overline{\mathbf{P}}}(\Omega) = \begin{bmatrix} P(\phi) & 0 \\ 0 & 0 \end{bmatrix} \delta(\theta - \pi/2), \tag{14}$$

leading to the simplification that the vector-dyadic formulation can be reduced to a scalar one. The PAS used is the multi-cluster truncated Laplacian distribution shown in Fig. 1.

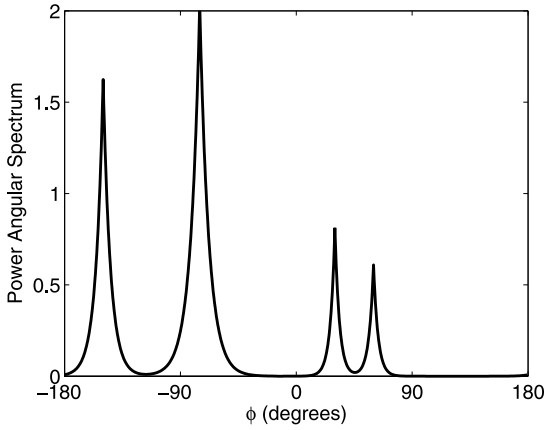

Fig. 1 Multi-cluster Laplacian power angular spectrum used in the generation of the optimal radiation patterns for a square aperture.

The computations assume Hertzian and half-wave wire dipoles. For Hertzian dipoles, $\mathbf{A}$ can be computed based on the closed-form radiation patterns, since the presence of an adjacent open-circuited Hertzian dipole will not impact the radiation pattern shape. For the half-wave dipoles, the radiation pattern for each element in the presence of all other elements terminated in an open circuit is computed using the NEC thin-wire moment method simulator [13]. Each wire has a diameter of 0.01 wavelengths, and 11 segments per dipole are used in the NEC moment method computation. For comparing the performance of the different antennas, we use the diversity gain assuming maximal ratio combining at the 1% probability level with a single isolated Hertzian dipole used as the reference antenna required in the computation [2].

Full characterization of this system requires including the mutual reactance of the array elements and the antenna terminations (i.e. matching network). Since the analysis obtained here can be used in conjunction with established network analysis techniques to include these impedance effects [14], we will concentrate here on the open-circuit characterization.

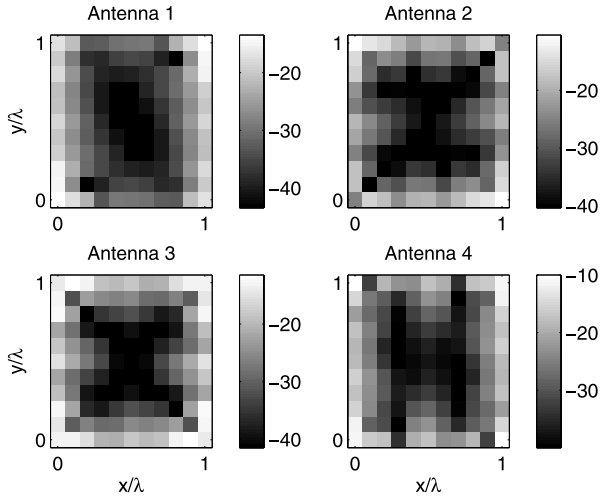

Fig. 2 The magnitude in dB of the current in the optimal four current distributions for a square aperture in an environment described by a multi-cluster Laplacian PAS using Hertzian dipoles.

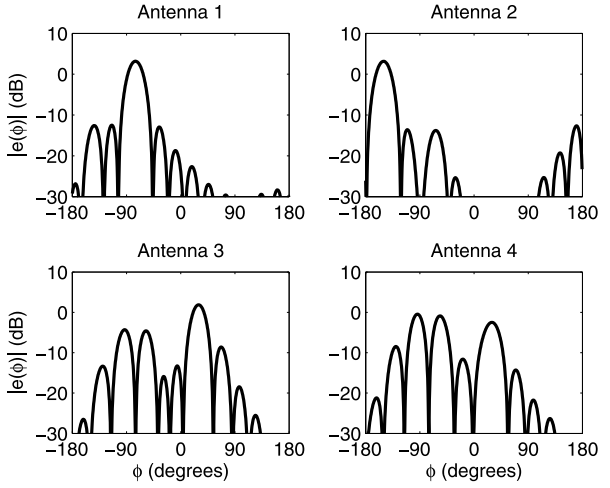

Fig. 3 Optimal four radiation patterns for a square aperture in an environment described by a multi-cluster Laplacian PAS using Hertzian dipoles.

Figures 2 and 3 show the current distributions and radiation patterns respectively for the optimal four antennas obtained using the Hertzian dipole array. Figure 4 shows the corresponding patterns for the half-wave dipole array, with the currents omitted for the sake of brevity since they, like the patterns, are very similar to those for the Hertzian dipole array. All computations assume a radiation efficiency of $\mu_n = 0.99$ (99%). The resulting diversity gains assuming the four largest communication modes are 22.9 dB for the Hertzian dipole array compared to 23.0 dB for the optimal half-wavelength dipole array. The results are nearly identical, with the slight improvement for the half-wavelength dipoles created by the unique open-circuit patterns exhibited by the coupled dipoles which produces some angle diversity in addition to the space diversity enabled by the array. However, it is important to re-emphasize that the performance of

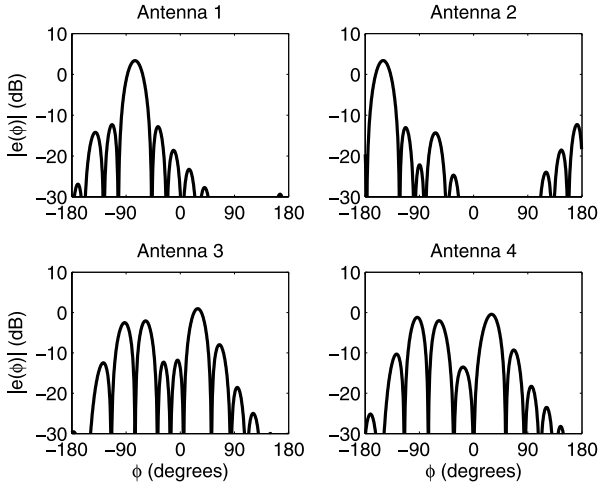

Fig. 4 Optimal four radiation patterns for a square aperture in an environment described by a multi-cluster Laplacian PAS using half-wavelength dipoles.

the coupled array of half-wave dipoles will typically degrade significantly if the antennas are attached to a sub-optimal matching network.

2.6 Optimal Reduced Array

Practical design likely involves using a significantly reduced set of elements. As a result, it is useful to understand the achievable performance of an optimal array consisting of a few elements compared to that for the optimal distribution based on the full array. To gain such an understanding, we use a genetic algorithm (GA) [6] to find the locations of four, six, or eight half-wave dipole antennas which maximize the diversity gain. In each case, the diversity gain is computed using the four dominant eigenfunctions computed for the array topology.

In each trial of the GA, a population consisting of 20 antenna arrays is initialized and analyzed for 125 generations. For each member of the population, the x or y coordinate for each dipole within the 1λ square aperture is represented by a single 7 bit gene. The population evolves using a steady state GA where the least-fit half of the parent population is replaced each generation. Parents are chosen using a tournament selection with 5 potential parents selected for each tournament. Once two parents are selected, crossover occurs on each individual gene (i.e. 8 unique crossovers for a 4-element array) with a probability of 0.7. To further improve convergence, every 10 generations, children are locally optimized with a probability of 0.01 using the Nelder-Mead simplex method. This process is repeated for 20 trials for each array size. Extensive evaluation of the GA parameters revealed that the final results are relatively insensitive to the actual parameter values.

Figure 5 plots the diversity gain as a function of generation number of the optimal array (chosen from among the 20 trials) for a simple truncated Gaussian PAS. This figure also shows the optimal bound (based on a full array

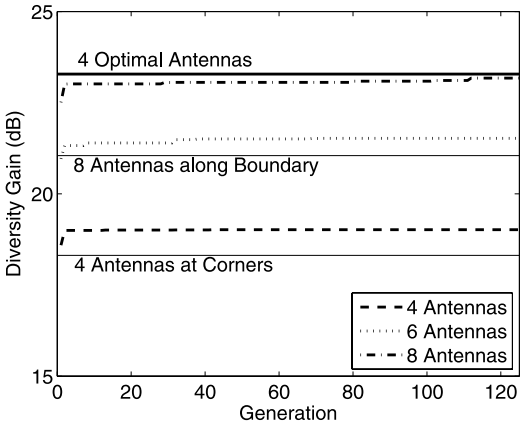

Fig. 5 The performance of arrays designed using genetic optimization compared to common array architectures.

of 11 × 11 half-wave dipoles) as well as the performance for four dipoles placed at the aperture corners and eight dipoles equally spaced around the aperture boundary (corners and side midpoints). It is interesting to note that for four elements, the genetically optimized array performance is similar to that for elements at the aperture corners. However, with eight elements, the performance differential for the genetically optimized and boundary arrays is substantial, with the performance of the optimal eight-element array approaching the achievable upper bound.

3. Optimal Antennas for Fixed Number of Elements

Section 2 has discussed the general problem of identifying optimal antenna characteristics in an average sense for time-varying channels when the antenna aperture size is constrained. A related problem is considering the optimal array configuration when the number of elements is fixed. Specifically, for a fast-fading environment where the channel remains constant only over one symbol time, it has recently been shown that increased transmit spatial correlation leads to improved capacity [7]. When the increased channel correlation is created by the propagation environment, such as when the multipath angle spread is reduced, this phenomenon is intuitive since this simply means that the transmit array can be used to better direct power into the preferred propagation directions. However, if the correlation arises due to decreased antenna spacing, the result is non-intuitive since very small spacing will degrade the array beamforming capability.

This section incorporates electromagnetic considerations into the study of correlated MIMO channels for highly mobile nodes to show that the increased performance observed with reduced antenna spacing can be associated with increased power radiated by the transmit array. The analysis further shows that when the formulation is altered to explicitly constrain the radiated power and limit superdirectivity, the capacity is maximized at a non-zero antenna spacing as expected.

3.1 Communications Model

Consider the communications model used in [15] where the channel is assumed constant for a block of T symbols but is statistically independent from the channel in any other block. If M and N represent the number of transmit and receive antennas, respectively, then during a block the complex baseband communication can be written as

$$\mathbf{X} = \sqrt{\frac{\rho}{M}}\mathbf{S}\mathbf{H} + \mathbf{W}, \tag{15}$$

where $\mathbf{X}$ is a $T \times N$ matrix of received symbols, $\mathbf{S}$ is a $T \times M$ matrix of transmitted symbols, $\mathbf{H}$ is the $M \times N$ channel transfer matrix, $\mathbf{W}$ is a $T \times N$ noise matrix whose elements are zero-mean, unit-variance i.i.d. complex Gaussian random variables, and ρ/M represents the single-input single-output (SISO) signal-to-noise ratio (SNR) with the factor of M indicating the division of the transmit power amongst the transmit antennas. Assuming a separable covariance structure (Kronecker model) [7], the channel matrix for a block can be expressed as

$$\mathbf{H} = \mathbf{K}_{\mathrm{t}}^{1/2}\mathbf{H}_{\mathrm{w}}\mathbf{K}_{\mathrm{r}}^{1/2}, \tag{16}$$

where $\mathbf{H}_{\mathrm{w}}$ is a $M \times N$ matrix of zero-mean, unit-variance i.i.d. complex Gaussian random variables. $\mathbf{K}_{\mathrm{t}}$ and $\mathbf{K}_{\mathrm{r}}$ are respectively the $M \times M$ transmit and $N \times N$ receive covariance matrices given by

$$\mathbf{K}_{\mathrm{t}} = \frac{1}{N}\mathrm{E}\left\{\mathbf{H}\mathbf{H}^{\dagger}\right\} \qquad \mathbf{K}_{\mathrm{r}} = \frac{1}{M}\mathrm{E}\left\{\mathbf{H}^{\dagger}\mathbf{H}\right\}. \tag{17}$$

To maintain unit average SISO gain, these matrices are normalized such that $\mathrm{Tr}\,[\mathbf{K}_{\mathrm{t}}] = M$ and $\mathrm{Tr}\,[\mathbf{K}_{\mathrm{r}}] = N$.

3.2 Mutual Information and Power Constraints

The mutual information for (15) assuming that the transmitter knows $\mathbf{K}_{\mathrm{t}}$ and the receiver knows $\mathbf{K}_{\mathrm{r}}$ is given by [7]

$$I(\mathbf{X};\mathbf{S}) = \int d\mathbf{S}\; p(\mathbf{S}) \int d\mathbf{X}\; p(\mathbf{X}|\mathbf{S}) \times \log\left\{\frac{p(\mathbf{X}|\mathbf{S})}{\int d\widehat{\mathbf{S}}\; p(\widehat{\mathbf{S}})p(\mathbf{X}|\widehat{\mathbf{S}})}\right\}, \tag{18}$$

where the probability of the received signal conditioned on the transmitted signal is

$$p(\mathbf{X}|\mathbf{S}) = \frac{\exp\left\{-\mathrm{Tr}\left[(\mathbf{I} + \frac{\rho}{M}\mathbf{K}_{\mathrm{r}} \otimes \mathbf{S}\mathbf{K}_{\mathrm{t}}\mathbf{S}^{\dagger})^{-1}\mathbf{x}\mathbf{x}^{\dagger}\right]\right\}}{\pi^{TN}\det\left[\mathbf{I} + \frac{\rho}{M}\mathbf{K}_{\mathrm{r}} \otimes \mathbf{S}\mathbf{K}_{\mathrm{t}}\mathbf{S}^{\dagger}\right]} \tag{19}$$

with $\mathbf{x}$ representing the elements of $\mathbf{X}$ stacked column-wise and $\otimes$ indicating the Kronecker product.

Determining the capacity of this system requires formulation of an appropriate power constraint. In most analyses, the power constraint assumes the form [7], [15]

$$\frac{1}{MT}\mathrm{E}\left\{\mathrm{Tr}\left[\mathbf{S}\mathbf{S}^{\dagger}\right]\right\} \le 1. \tag{20}$$

This constraint limits the sum of the squares of the currents (or voltages) applied to the transmit antennas which for widely-spaced antennas (with a diagonal impedance matrix) effectively limits the power radiated by the array. However, for closely-spaced (coupled) antennas, the coherent addition of the radiated fields can result in large radiated power when (20) is used in the capacity formulation.

To address this issue, we will again explore the case when the radiated power is explicitly constrained using

$$\frac{1}{MT}\mathrm{E}\left\{\mathrm{Tr}\left[\mathbf{S}\widehat{\mathbf{A}}\mathbf{S}^{\dagger}\right]\right\} \le 1, \tag{21}$$

where $\widehat{\mathbf{A}} = \mathbf{A} + \mathbf{R}_L$. In this case, however, we will normalize $\mathbf{A}$ to have unity down the diagonal so that $\widehat{\mathbf{A}} \to \mathbf{I}$ as the antenna spacing increases (for $\mu_n = 1$), revealing that (21) represents a generalization of (20).

The capacity computation under the radiated power constraint is simplified by manipulating the mutual information expression. Using the substitution $\widetilde{\mathbf{S}} = \mathbf{S}\widehat{\mathbf{A}}^{1/2}$ in (19) and (21) leads respectively to

$$p(\mathbf{X}|\widetilde{\mathbf{S}}) = \frac{\exp\left\{-\mathrm{Tr}\left[(\mathbf{I} + \frac{\rho}{M}\mathbf{K}_{\mathrm{r}} \otimes \widetilde{\mathbf{S}}\widetilde{\mathbf{K}}_{\mathrm{t}}\widetilde{\mathbf{S}}^{\dagger})^{-1}\mathbf{x}\mathbf{x}^{\dagger}\right]\right\}}{\pi^{TN}\det\left[\mathbf{I} + \frac{\rho}{M}\mathbf{K}_{\mathrm{r}} \otimes \widetilde{\mathbf{S}}\widetilde{\mathbf{K}}_{\mathrm{t}}\widetilde{\mathbf{S}}^{\dagger}\right]}, \tag{22}$$

$$\frac{1}{MT}\mathrm{E}\left\{\mathrm{Tr}\left[\widetilde{\mathbf{S}}\widetilde{\mathbf{S}}^{\dagger}\right]\right\} \le 1, \tag{23}$$

where $\widetilde{\mathbf{K}}_{\mathrm{t}} = \widehat{\mathbf{A}}^{-1/2}\mathbf{K}_{\mathrm{t}}\widehat{\mathbf{A}}^{-1/2}$. This substitution therefore transforms our problem into a form identical to that for the conventional power constraint. This means that we can leverage the prior work for the conventional power constraint to state that under the radiated power constraint (a) capacity is maximized by signaling on the dominant eigenvector of $\widetilde{\mathbf{K}}_{\mathrm{t}}$ and (b) the capacity increases when the dominant eigenvalue of $\widetilde{\mathbf{K}}_{\mathrm{t}}$ increases. In the remainder of this paper, we will use the notation of (18)–(20), understanding that the computational approach applies to the capacity computation under the radiated power constraint using the appropriate variable substitutions.

3.3 Capacity

With the mutual information expression (18) and power constraint (20), the distribution for $\mathbf{S}$ which achieves capacity is $\mathbf{S} = \mathbf{\Phi}\mathbf{V}\mathbf{U}_{\mathrm{t}}^{\dagger}$, where $\mathbf{\Phi}$ is a $T \times T$ isotropically distributed matrix and $\mathbf{U}_{\mathrm{t}}$ is the $M \times M$ unitary matrix of eigenvectors of $\mathbf{K}_{\mathrm{t}}$ [7]. The $T \times M$ matrix $\mathbf{V}$ has non-zero entries only on the main diagonal. Computation of the capacity requires determination of the distribution of these $\min(T, M)$ real, non-negative diagonal entries of $\mathbf{V}$, which can be accomplished using the Blahut-Arimoto algorithm [16].

3.4 Computational Results

We are now prepared to explore the impact of array element spacing on the capacity of fast-fading MIMO channels

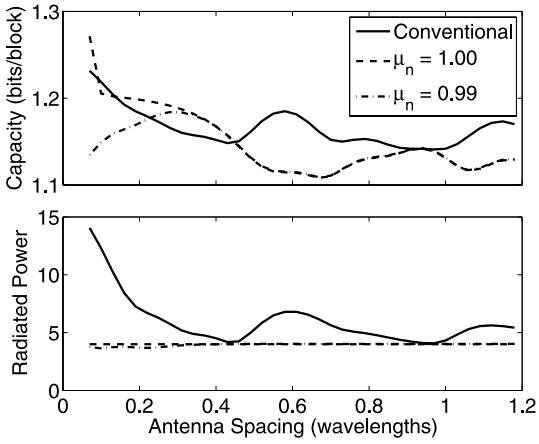

Fig. 6 The capacity and power radiated for a single channel realization using conventional and radiated power constraints.

where $T = 1$. Each antenna is a uniform linear array (ULA) of half-wave dipole elements. We will use the result from previous studies that since the half-wave dipole is approximately a minimum scattering antenna, the radiation pattern of a half-wave dipole in the presence of adjacent elements terminated in an open circuit is very similar to that of the dipole radiating in isolation [10]. Closed-form expressions are used to construct the coupled element resistance matrix [17].

We represent the environment using a well-established path-based stochastic propagation model [18] and assume that the multipath propagation is confined to the horizontal plane. The full covariance matrix for this scenario can be constructed from

$$\begin{aligned} K_{mn,pq} &= \mathrm{E}\left\{H_{mn}H_{pq}^{*}\right\} \\ &= \sum_{\ell} |\beta_{\ell}|^2 e^{jkd_{\mathrm{t},mp}\cos\phi_{\mathrm{t},\ell}} e^{jkd_{\mathrm{r},nq}\cos\phi_{\mathrm{r},\ell}}, \end{aligned} \tag{24}$$

where β_{ℓ}, $\phi_{\mathrm{t},\ell}$, $\phi_{\mathrm{r},\ell}$ represent the complex gain, departure angle, and arrival angle respectively of the ℓth multipath, $d_{\mathrm{t},mp}$ is the distance between the mth and pth transmit antennas, $d_{\mathrm{r},nq}$ is the distance between the nth and qth receive antennas, and the expectation is taken by moving the arrays along the x axis. A Kronecker approximation to this covariance can then be generated using (17) to obtain

$$K_{\mathrm{t},ij} = \sum_{n=1}^{N} \frac{K_{in,jn}}{N} \qquad K_{\mathrm{r},ij} = \sum_{m=1}^{M} \frac{K_{mj,mi}}{M}. \tag{25}$$

We first consider a single realization of the stochastic propagation model for a system with $T = 1$, $M = 4$, and $N = 1$. Figure 6 plots the capacity for this system as a function of the transmit ULA element spacing for both power constraints. For the radiated power constraint, antenna efficiencies of $\mu_n = 1$ and $\mu_n = 0.99$ are considered. A plot of the average radiated power, computed from $(1/T)\mathrm{E}\left\{\mathrm{Tr}\left[\mathbf{S}\mathbf{A}\mathbf{S}^{\dagger}\right]\right\}$ with $\mu_n = 1$, is also included. The first key observation from this plot is that when the conventional

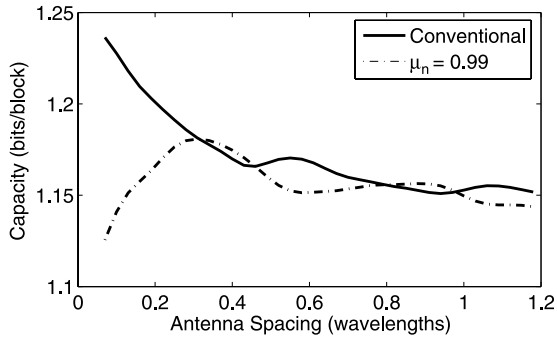

Fig. 7 The average capacity for 100 random channel realizations using conventional and radiated power constraints.

power constraint is used, the capacity increases monotonically as the array spacing decreases below about 0.4 wavelengths, confirming the findings of [7]. However, this result is non-intuitive, since under these circumstances optimal transmission is performed using the dominant eigenvector of $\mathbf{K}_t$, which means that any capacity increase must be a result of beamforming gain (as opposed to multiplexing gain) as the transmit array more effectively directs power into the preferred propagation directions. This phenomenon should begin to degrade as the spacing becomes narrow and the array beamforming capability is compromised. The radiated power results in Fig. 6 explain this unexpected observation, revealing that this capacity increase is accompanied by (and due to) a commensurate increase in radiated power.

When the radiated power is explicitly constrained in the computation, the results for the lossless elements ($\mu_n = 1$) again show that the capacity increases for decreasing element spacing due to the presence of array supergain. When only a small amount of loss is incorporated into the computation ($\mu_n = 0.99$), this supergain phenomenon is significantly reduced since the large currents required to achieve the radiated power level with a supergain excitation result in high ohmic losses. In this case, the performance is maximized when the element spacing is approximately 0.3 wavelengths. This result is physically satisfying, since small transmit element spacing reduces the beamforming capability of the array. On the other hand, large element spacing results in grating lobes which waste power by radiating into directions that do not provide a strong propagation path to the receiver.

While exploring the performance in a single channel is instructive, it is perhaps more practical to consider the average behavior over an ensemble of such channels. For each of 100 random realizations of the model, the transmit covariance for a system with $M = 4$ and $N = 1$ was constructed using (24) and (25), and subsequently the capacity was computed using the conventional and radiated power constraints. Figure 7 plots the average capacity resulting from these simulations. Essentially, these results confirm that the findings already discussed apply more generally than to the single propagation environment considered in Fig. 6.

4. Conclusion

This paper has explored methods for determining the optimal antenna array radiation characteristics based on stochastic characteristics of the propagation environment at either the transmit or receive end of the link under two different scenarios. Under the assumption that the antennas reside in a fixed aperture, the paper has demonstrated optimal current distributions and radiation patterns given an average description of the propagation channel, making the results applicable to time-variant channels characteristic of mobile nodes. It has also shown that near-optimal performance can be obtained with reasonable complexity using numerically optimized practical designs. The paper has also explored the impact of element spacing for a fixed number of elements and fast fading channels with spatial correlation. In this case, the paper demonstrated that previously-reported performance gains associated with decreased element spacing in this scenario result from increased power radiated by the transmit array, and that when this power is explicitly constrained, optimal performance occurs when the array spacing is close to that for a conventional array design (around 0.3 wavelengths).

References

[1] M.A. Jensen and J.W. Wallace, "A review of antennas and propagation for MIMO wireless communications," IEEE Trans. Antennas Propag., vol.52, no.11, pp.2810–2824, Nov. 2004.

[2] O. Nørklit, P.D. Teal, and R.G. Vaughan, "Measurement and evaluation of multi-antenna handsets in indoor mobile communication," IEEE Trans. Antennas Propag., vol.49, no.3, pp.429–437, March 2001.

[3] R.G. Vaughan and J.B. Andersen, "Antenna diversity in mobile communications," IEEE Trans. Veh. Technol., vol.VT-36, no.4, pp.147–172, Nov. 1987.

[4] S. Nordebo, M. Gustafsson, and G. Kristensson, "On the capacity of the free space antenna channel," Proc. 2006 IEEE Antennas and Propag. Society Intl. Symp., pp.3105–3108, Albuquerque, NM, July 2006.

[5] M.A. Jensen and J.W. Wallace, "Antenna-independent capacity bound of electromagnetic channels," Proc. 2005 IEEE Antennas and Propag. Society Intl. Symp., pp.317–320, Washington, DC, July 2005.

[6] Y. Rahmat-Samii and E. Michielssen, Electromagnetic Optimization by Genetic Algorithm, John Wiley & Sons, New York, NY, 1999.

[7] S.A. Jafar and A. Goldsmith, "Multiple-antenna capacity in correlated Rayleigh fading with channel covariance information," IEEE Trans. Wireless Commun., vol.4, no.3, pp.990–997, May 2005.

[8] K. Mardia, J. Kent, and J. Bibby, Multivariate Analysis, Academic Press, 1980.

[9] J.A. Kong, Electromagnetic Wave Theory, John Wiley & Sons, 1990.

[10] N.W. Bikhazi and M.A. Jensen, "The relationship between antenna loss and superdirectivity in MIMO systems," IEEE Trans. Wireless Commun., vol.6, no.5, pp.1796–1802, May 2007.

[11] M. Uzsoky and L. Solymar, "Theory of super-directive linear antennas," Acta Physica Hungarica, vol.6, no.2, pp.185–205, 1956.

[12] T.K. Moon and W.C. Stirling, Mathematical Methods and Algorithms for Signal Processing, Prentice-Hall, 2000.

[13] G.J. Burke and A.J. Poggio, "Numerical electromagnetics code

(NEC)-method of moments," Tech. Rep. NOSC Tech. Document 116, Lawrence Livermore Laboratory, Jan. 1981.
[14] M.L. Morris and M.A. Jensen, "Network model for MIMO systems with coupled antennas and noisy amplifiers," IEEE Trans. Antennas Propag., vol.53, no.1, pp.545–552, Jan. 2005.
[15] T.L. Marzetta and B.M. Hochwald, "Capacity of a mobile multiple-antenna communication link in Rayleigh flat fading," IEEE Trans. Inf. Theory, vol.45, no.1, pp.139–157, Jan. 1999.
[16] R.E. Blahut, "Computation of channel capacity and rate-distortion functions," IEEE Trans. Inf. Theory, vol.IT-18, no.4, pp.460–473, July 1972.
[17] C.A. Balanis, Antenna Theory: Analysis and Design, Wiley, 1997.
[18] Q.H. Spencer, B.D. Jeffs, M.A. Jensen, and A.L. Swindlehurst, "Modeling the statistical time and angle of arrival characteristics of an indoor multipath channel," IEEE J. Sel. Areas Commun., vol.18, no.3, pp.347–360, March 2000.

Michael A. Jensen received the B.S. (summa cum laude) and M.S. degrees in Electrical Engineering from Brigham Young University (BYU) in 1990 and 1991, respectively, and the Ph.D. in Electrical Engineering at the University of California, Los Angeles (UCLA) in 1994. From 1989 to 1991 he was a graduate researcher in the Lasers and Optics Laboratory at BYU, during which time he received a National Science Foundation Graduate Fellowship. From 1991 to 1994, he was a graduate student researcher in the Antenna Laboratory at UCLA. Since 1994, he has been at the Electrical and Computer Engineering Department at BYU where he is currently a Professor and Department Chair. His research interests include antennas and propagation for communications, microwave circuit design, numerical electromagnetics, and optical fiber communications. He was eleveated to IEEE Fellow in 2008.

Britton T. Quist received a B.S. and an M.S. in electrical engineering from Brigham Young University (BYU) in 2005 and 2007 respectively. His research interests are in MIMO arrays. From 2005 to 2007, he worked as a research assistant in the Wireless Communications Laboratory at BYU. He has been employed by IMSAR since 2007.

Nicolas W. Bikhazi received the B.S. and Ph.D. degrees in electrical engineering from Brigham Young University (BYU) in 2003 and 2006 respectively. For the summers of 2001 and 2002 he was an intern at Hewlett-Packard. From 2003 to 2006 he was a research assistant at BYU. In 2006 he began working for Sandia National Laboratories. His research interests are in wireless and optical MIMO communication systems.